Geophysical Research Letters

RESEARCH LETTER
10.1029/2024GL111264

Unprecedented Summer Phytoplankton Bloom in the Ross Sea

Esther Portela[1,2], Meredith G. Meyer[1,3], Karen J. Heywood[1], and Walker O. Smith[3,4]

[1]Centre for Ocean and Atmospheric Sciences (COAS), School of Environmental Sciences, University of East Anglia, Norwich, UK, [2]Now at Laboratoire D'Oceanographie Physique et Spatiale (LOPS), University Brest, CNRS, IRD, Ifremer, Plouzane, France, [3]Virginia Institute of Marine Science, College of William & Mary, Gloucester Point, VA, USA, [4]Now at School of Oceanography, Shanghai Jiao Tong University, Shanghai, China

Key Points:

- Chlorophyll concentrations more than six times greater than previously reported, were observed in the southern Ross Sea in summer 2022–2023
- Our observations are consistent with a large ice-edge bloom associated with an anomalously ice-covered summer
- Late sea-ice melt likely provided the perfect combination of iron release, sufficient light, and high stratification that fueled the bloom

Supporting Information:

Supporting Information may be found in the online version of this article.

Correspondence to:

E. Portela,
esther.portela_rodriguez@ird.fr

Citation:

Portela, E., Meyer, M. G., Heywood, K. J., & Smith, W. O. (2025). Unprecedented summer phytoplankton bloom in the Ross Sea. *Geophysical Research Letters*, *52*, e2024GL111264. https://doi.org/10.1029/2024GL111264

Received 11 JUL 2024
Accepted 9 DEC 2024

Abstract High-resolution glider sampling in the southwestern Ross Sea revealed an extensive phytoplankton bloom in austral summer 2022–2023 that persisted for over one month and extended through the upper 100 m of the water column. The temporal mean euphotic-zone chlorophyll concentration was 20.3 $\pm$8.5 μg L^{-1}, six to nine times higher than average summer Ross Sea concentrations. The bloom was likely initially dominated by *Phaeocystis*, favored over diatoms due to low light and high iron availability. Our observations are consistent with an ice-edge bloom likely fueled by iron supply and enhanced stratification from late sea-ice melt during an anomalously high ice-covered summer. Photoacclimation to particularly low light conditions might have enhanced Chl-a fluorescence. In the Ross Sea, the most productive region in the Southern Ocean, understanding the drivers of this extreme bloom is crucial for predicting potential impacts of the changing climate on primary production rates and carbon sequestration.

Plain Language Summary During austral summer 2022–2023,ocean gliders revealed extreme levels of phytoplankton abundance in the Ross Sea, with chlorophyll concentrations six to nine times higher than previously reported. Variations in light, water column stability, and phytoplankton species governed the fluctuations in chlorophyll concentration throughout the season. We suggest this extreme bloom is associated with sea-ice melt, triggered by unusually high and late ice cover during that summer. High chlorophyll levels persisted for over a month and penetrated to 100 m. Given the Ross Sea's importance as a productive area in the Southern Ocean, understanding these blooms drivers is crucial for predicting consequences of changing climate on the carbon absorption by the ocean and ecosystems.

1. Introduction

The Ross Sea is the most productive Southern Ocean region, and it accounts for up to 27% of the estimated Southern Ocean biological CO_2 uptake (Arrigo et al., 2008). Phytoplankton growth varies spatially and temporally in the Ross Sea as a function of sea-ice concentration (SIC), vertical mixing depth, solar irradiance, and iron concentrations (Arrigo et al., 1998; McGillicuddy et al., 2015; Smith et al., 2000). The latter two factors limit primary production in Antarctic regions including the continental shelf waters of the Ross Sea polynya (Sedwick et al., 2011).

Winter vertical mixing provides the largest iron source to the water column. However, extensive sea-ice cover reduces irradiance available for phytoplankton growth until austral spring. In late October, as incoming solar irradiance increases, sea ice melts, increasing vertical stratification and providing an additional iron source in Antarctic shelf waters (Sedwick & Ditullio, 1997). This accelerates the growth of phytoplankton, which reaches maximum biomass in mid- to late-December (Smith et al., 2000). As the growing season progresses, the available iron is progressively consumed until reaching limiting conditions (McGillicuddy et al., 2015) following the biomass peak (Arrigo & van Dijken, 2003; Smith et al., 2011). Secondary iron sources, such as lateral advection (McGillicuddy et al., 2015; Salmon et al., 2020), can maintain the bloom later in the growing season (early to mid-January), while glacial meltwater is a minor source in this region (McGillicuddy et al., 2015).

The composition of summer blooms is determined by physical and biogeochemical conditions. As the Ross Sea polynya expands in spring, deep mixed layers (i.e., low stratification) reduce the irradiance available to phytoplankton for photosynthesis (Smith & Jones, 2015), and iron concentrations are elevated. In these conditions, phytoplankton are initially dominated by the haptophyte *Phaeocystis antarctica* (Goffart et al., 2000; Smith &

Trimborn, 2024), with high-iron and low-light requirements. Later in the bloom, the progressive iron-limitation and increasing irradiance favor diatom growth over *Phaeocystis* (Arrigo et al., 1999; DiTullio et al., 2003; Ryan-Keogh & Smith, 2021; Smith, Ainley, et al., 2014; Smith & Kaufman, 2018; Strzepek et al., 2002). Diatoms typically dominate later in the season in more stratified waters, such as retreating sea-ice edges (Arrigo et al., 1998; Goffart et al., 2000).

Although the factors impacting phytoplankton growth and composition have been identified, the drivers of the large interannual variability of the regional bloom intensity are still uncertain. The interaction of these drivers in different environmental conditions (SIC, wind intensity, temperature and salinity, etc.) and their synergistic or antagonistic effects on phytoplankton blooms remain poorly understood. Some of these drivers are either being, or projected to be, altered by climate change. For instance, sea-ice extent has increased in the Ross Sea over recent decades (Comiso et al., 2011; Yuan et al., 2017), while projections of future mixed layer depth or nutrient supply are uncertain (Boyd, 2002). Changes in SIC will impact ice melt timing, thus, iron supply, light penetration and water column stability, affecting oceanic productivity, phytoplankton composition, and carbon sequestration (Rozema et al., 2017). Therefore, there is an urgent need for better understanding of the relative roles of different phytoplankton bloom controls in highly productive regions such as the Ross Sea. Our high-resolution physical and biogeochemical glider data combined with historical satellite-derived data sets allowed us to investigate the influence of some of these controls on the characteristics and intensity of an extreme phytoplankton bloom observed in the Ross Sea during summer 2022–2023. Our results suggest a key role for SIC and stratification in the development and evolution of the bloom.

2. Data and Methods

2.1. Glider Data

Two profiling ocean gliders (Seagliders SG613 and SG676) were deployed from the fast ice adjacent to the Ross ice shelf near Cape Crozier (Figure 1). They sampled the southwestern Ross Sea within 169.5–172.3°W and 77.4–76.4°S between 29 November 2022, when SG613 was deployed, and 4 December 2022, when SG676 was deployed, to 18 January 2023, when both gliders were recovered by *RVIB Nathaniel B. Palmer* (Figure 1b). SG613 and SG676 collected 774 and 688 profiles, respectively, where each profile (taking typically 1.5 hr) is either an ascent or descent, with its mean time assigned. The glider data set can be found in Portela et al. (2024).

The gliders carried sensors for temperature, salinity (Seabird CT sail), dissolved oxygen (Aanderaa 4330 optode), Chl-a fluorescence (a proxy for phytoplankton biomass), and optical backscatter (OBS) at 470 and 700 nm (Seabird Scientific Wetlabs Triplet ECOpuck). SG613 also carried a photosynthetically active radiation (PAR) sensor. Glider sensors were factory-calibrated before the deployment. Data were processed using the UEA Seaglider Toolbox (bitbucket.org/bastienqueste/uea-seaglider-toolbox, Queste et al. (2014)), optimizing the hydrodynamic flight model (Frajka-Williams et al., 2011) and correcting conductivity for thermal hysteresis (Garau et al., 2011). The accuracy of glider fluorescence was ensured via cross-calibration of fluorescence measurements from both gliders and the CTD rosette at the recovery stations. These showed good agreement (Figure S1 in Supporting Information S1). Discrete chlorophyll samples were collected via the CTD rosette on glass fiber filters upon glider recovery and analyzed fluorometrically (Knap et al., 1996) aboard the Palmer. Glider fluorescence was converted to Chl-a via a linear regression of the last glider profile with bottle Chl-a samples (Chl-a = 0.962Fluorescence +0.406, $R^2 = 0.97$, $p < 0.01$, $n = 18$ sample points, where p is the probability of rejecting the null hypothesis); the Fluorescence:Chl-a ratio was nearly 1:1 (Figure S2b in Supporting Information S1). Discrete particulate organic carbon (POC) samples were likewise collected from the recovery CTD cast, filtered through combusted glass fiber filters and analyzed in the laboratory by pyrolysis (Gardner et al., 2000). Conditions at the ice-shelf edge did not allow collection of data or samples for calibration during deployment. Conversion procedures from fluorescence to Chl-a and from OBS to POC (Figures S1 and S2 in Supporting Information S1), and estimation of Chl-a from the diffuse attenuation coefficient (k_d) using PAR (Figure S3 in Supporting Information S1), are detailed in Supporting Information S1.

2.2. Other Data Sets

Daily SIC derived from the satellite microwave radiometer AMSR2 (Spreen et al., 2008) at 3.125 km resolution were used to analyze conditions during our survey. Monthly mean SIC between 1992 and 2023 at 25 km resolution from NOAA/NSIDC (National Snow and Ice Data Center) (Meier et al., 2021) were used to compute long-

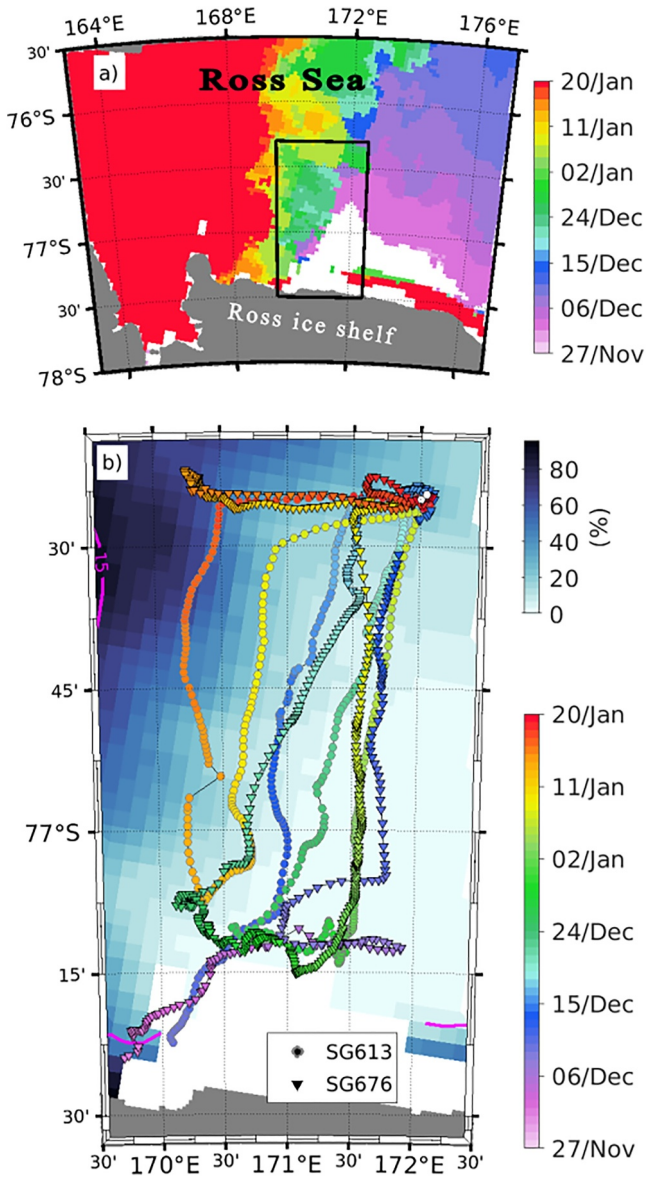

Figure 1. (a) Study location on the Ross Sea continental shelf. Colors represent last date when SIC equal or above 15% was observed (proxy of sea-ice melt timing). White indicates areas where SIC was always lower than 15% (including the ice-shelf) and red indicates areas where sea-ice melt occurred after 20 January 2023. Black rectangle shows glider sampling area. (b) Spatio-temporal sampling of SG613 (circles) and SG676 (triangles), with symbols showing mean profile location colored by time. Blue shading shows mean SIC in December 2022. White shows unavailability of SIC data including the ice shelf. Magenta contour is 15% mean SIC in January 2023. White symbols in the northeast corner show glider recovery locations.

term SIC anomalies. From hourly 10-m wind speed at 0.25° × 0.25° resolution from the ECMWF atmospheric reanalysis ERA5 Hersbach et al. (2018)), we computed monthly averages between 1992 and 2023. We assessed monthly mean level-3 Satellite AQUA-MODIS PAR data at 4.6 km resolution between 2002 and 2023 from the Ocean Biology Processing Group (NASA/GSFC/OBPG) (NASA Ocean Biology Processing Group, 2018). To obtain long-term timeseries for our study region of SIC, wind speed and PAR (variables involved in phytoplankton growth), we computed the spatial median approximately within the region covered by the gliders (longitude between 168° and 173°W and latitude between 76° and 77.5°S).

2.3. Data Analysis

All glider data were interpolated onto a 1 m vertical grid. Mixed layer depths were computed as the depth of a $\Delta\sigma$ threshold of 0.01 kg m^{-3} from a reference depth of 10 m (Smith, 2022) and set to 5 m (the midpoint between the surface and the reference depth) when shallower than the reference depth. For clarity of visualizing isopycnals, we gridded density in bins of 5 hr in time and 3 m vertically. The euphotic depth (E_z), above which light intensity is sufficient to support photosynthesis, was calculated for each SG613 profile as the depth of 1% of the maximum instantaneous PAR measured by the glider. Stratification through E_z $(\Delta\sigma_{(E_z)})$ was approximated as the difference between the density at E_z and that at 10 m depth for each profile.

Non-photochemical quenching (NPQ), the reduction in chlorophyll fluorescence in surface waters under super-saturating irradiance (Müller et al., 2001), was corrected in all glider profiles, as the Ross Sea photoperiod was 24 hr. We selected the depth range with a nearly constant POC:Fluorescence ratio (POC:F) for each profile (Figure S1a in Supporting Information S1), and then used the vertical mean of this ratio $(\overline{R})$ to re-estimate fluorescence from the base of the 5 µmol photon m^{-2} s^{-1} isolume (5iL) to the surface as: $F_{(0:5iL)} = POC_{(0:5iL)}/\overline{R}$. This correction uses a light threshold following the recommendations of Xing et al. (2018). The 5iL value was empirically determined to be the most effective at delimiting the NPQ depth. To perform more efficient NPQ correction, vertical smoothing was applied to the Chl-a and POC profiles by computing a weighted linear least squares regression over 5-m windows of the glider profiles for each variable.

We computed euphotic-layer means of Chl-a, POC and their ratio (POC:Chl-a) over E_z of each profile. We applied temporal smoothing using weighted linear least squares regression with a 16-profile (≈24 hr) window to remove small-scale variability and diurnal signals that were not the focus of this study. Pairs of variables were correlated using smoothed, detrended euphotic-layer averages. Temporal averages of mean euphotic-depth Chl-a, POC, and their ratio were computed. Lower POC:Chl-a ratios are associated with dominance of *Phaeocystis*, while higher ratios indicate a taxonomic shift toward diatom dominance (Smith et al., 2000; Smith & Kaufman, 2018).

3. Results and Discussion

3.1. Biogeochemical Characterization of the 2022–2023 Bloom

Since both gliders exhibited consistent observations between all measured variables, we illustrate the temporal evolution of the vertical structure of the oceanographic conditions during the bloom using glider SG613 (Figure 2); equivalent time series for SG676 are shown in Figure S4 in Supporting Information S1. The

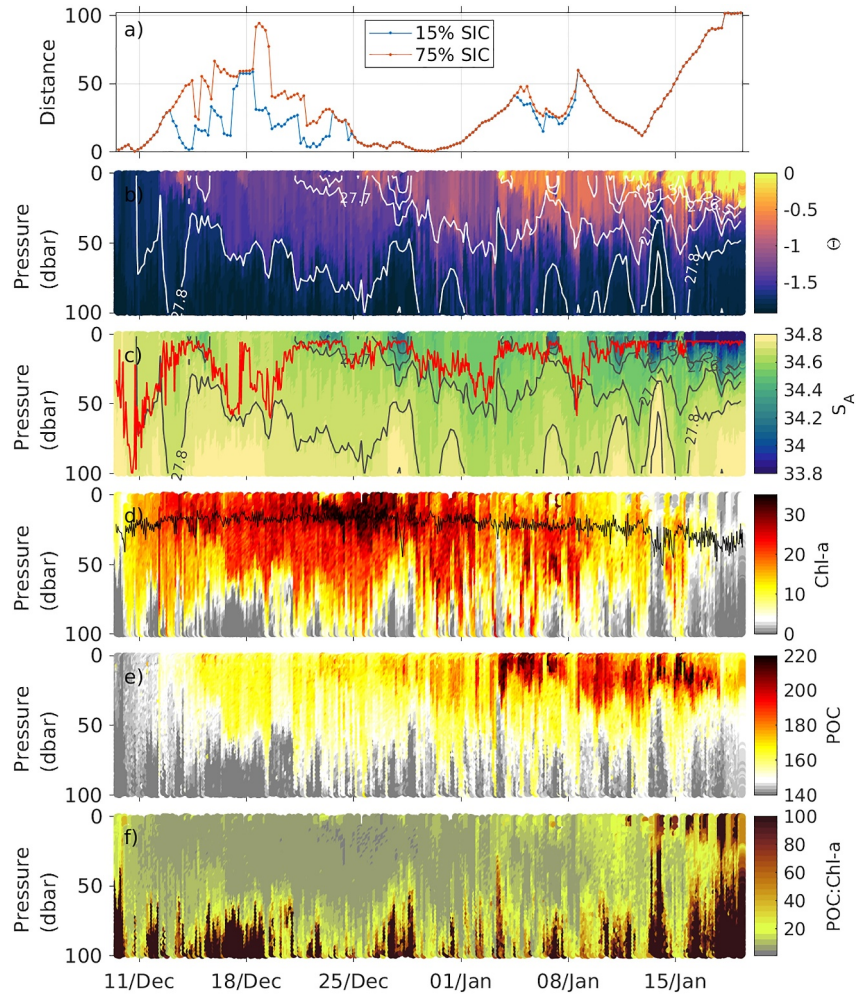

Figure 2. Time series of properties from glider SG613. (a) Closest distance (km) from glider location to the 15% (blue) and 75% (red) SIC contours. (b) Conservative temperature (°*C*), (c) Absolute salinity (g kg^{-1}), (d) Chl-a concentration (μg L^{-1}), (e) POC (μg L^{-1}) and (f) POC:Chl-a ratio. Thin white or gray contours represent isopycnals. Red line in (c) is mixed layer depth. Black line in (d) is euphotic depth. For equivalent figure for SG676 see Figure S4 in Supporting Information S1.

southwestern Ross Sea still had substantial sea-ice cover during our survey (Figures 1 and 2a). The gliders revealed progressive warming (Figure 2b) and freshening (Figures 2c and 3b) of the surface layer due to increasing solar radiation and sea-ice melt that enhanced upper water-column stratification (Figure 3d). The mixed layer reached a maximum depth of 80 m on 11 December and shoaled substantially over time. The shallowest mixed layers (<10 m) were observed from 10 January until the end of sampling as the upper water column became fresher (Figures 2c and 3b). The average mixed layer depth during our survey was 15 m, less than the regional climatology (Smith, 2022) and than in previous glider surveys in the same month and region using the same criterion (Kaufman et al., 2014). Mesoscale features identified from isopycnal doming (Figures 2b and 2c) and from steric height anomalies (not shown), further altered the vertical stability of the water column.

The most striking feature of the glider survey was the presence of very large (more than 25 μg L^{-1}) and sustained Chl-a concentrations that extended below E_z (black line in Figure 2d) and the mixed layer (red line in Figure 2c) for more than one month (Figure 2d). The observed Chl-a distribution is consistent with a bloom that started before the glider deployment (see Figure S4 in Supporting Information S1 for glider SG676), intensified until the end of December, and rapidly dissipated through mid January (Figures 2d and 3a). Previous glider surveys measuring the summer bloom in this region exhibited maximum Chl-a concentrations of about 7 μg L^{-1} in 2010–2011 (Kaufman et al., 2014; Queste et al., 2014), and around 8 μg L^{-1} in 2012–2013 (Jones & Smith, 2017). In

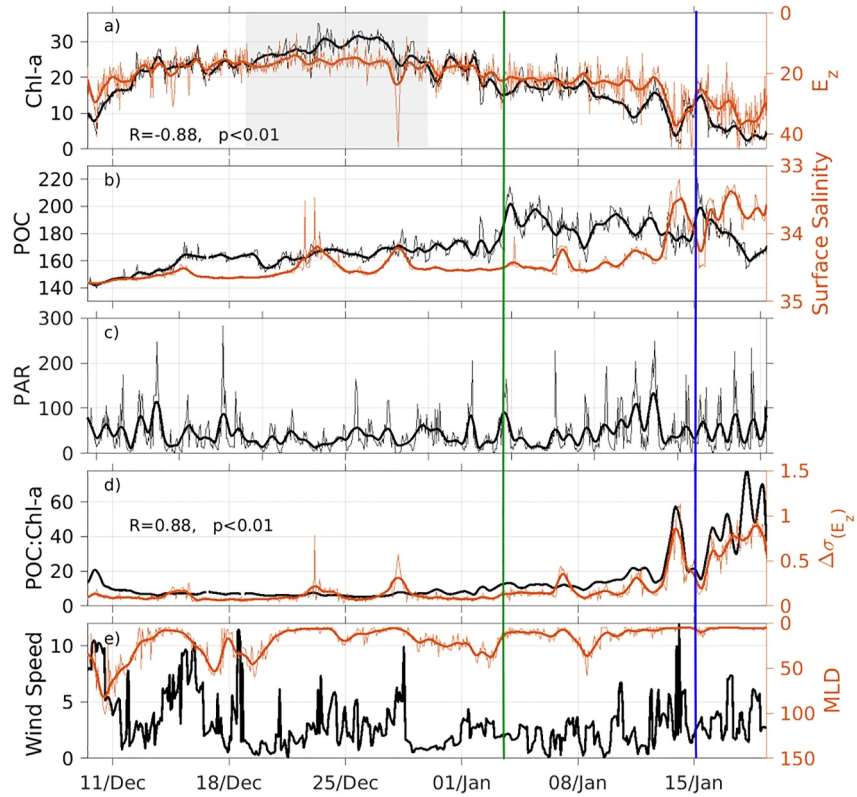

Figure 3. Time series of ocean properties, both full-resolution, every glider profile (thin lines), and smoothed (thick lines). (a) Mean euphotic-zone Chl-a (μg L^{-1}) (black) and euphotic depth (E_z, m, orange). (b) Mean euphotic-zone POC (μg L^{-1}) (black) and surface salinity (g kg^{-1}, orange). (c) PAR (μ mol photon m^{-2} s^{-1}) at 1 m. (d) Mean euphotic zone C:Chl-a ratio (black) and stratification through the euphotic depth (kg m^{-3}, orange). (e) Wind speed $\left(\text{m s}^{-1}\right)$ (black) and mixed layer depth (m) (orange). Green and blue lines delimit three different periods according to mean euphotic-zone POC.

contrast, using the same type of optical sensor, we observed maximum concentrations above 30 μg L^{-1} between 20–30 December 2022 (Figure 2d). The temporal mean of the average euphotic-zone Chl-a was 20.3 ± 8.5 μg L^{-1} (where standard deviation represents temporal variability), ranging between 5 and 35 μg L^{-1} (Figure 3a). Analysis of numerous Ross Sea ship campaigns conducted between 1983 and 2006 yielded an average euphotic-zone Chl-a of 2.9 ± 2.7 μg L^{-1}, with a maximum observed concentration of 19.1 μg L^{-1} (Smith, 2022). Climatological mean Chl-a at 15 m from 42 cruises carried out in the Ross Sea continental shelf between 1967 and 2016 was 3.2 ± 1.8 μg L^{-1} in December and 2.2 ± 1.0 μg L^{-1} in January (Smith & Kaufman, 2018).

There is a strong negative correlation ($R = -0.88$, p<0.01, Figure 3a) between the smoothed euphotic depth and mean euphotic-zone Chl-a, which is consistent with increased Chl-a absorbing more light and restricting its vertical penetration. This strong correlation weakened during the maximum Chl-a period (20–30 December, Figure 3a). Relatively low PAR at 1 m was observed then (mean 34 ± 28 μ mol photon m^{-2} s^{-1} c f. deployment mean 45 ± 44 μ mol photon m^{-2} s^{-1}, Figure 3c, Figure S3 in Supporting Information S1), possibly due to shading by large *Phaeocystis* colonies. This suggests that high Chl-a concentrations are present from the ocean surface, maybe trapped by the strong near-surface stratification (Figures 2b and 2c and 3d).

Mean POC and Chl-a concentrations do not co-vary (Figures 2d and 2e) and both follow previously reported temporal patterns for this region (Kaufman et al., 2014; Meyer et al., 2022; Smith, 2022). POC concentrations were greatest in January, with maxima in the upper 30 m (Figures 2e and 3b). The temporal mean euphotic-zone POC was 170 ± 14 μg L^{-1}, lower than climatological mixed-layer averages (254 ± 127 μg L^{-1} in December and 261 ± 66 μg L^{-1} in January) computed for the Ross Sea continental shelf over depth ranges similar to our euphotic zone averages (Smith & Kaufman, 2018). POC concentrations were also lower in summer 2022–2023

than in a previous glider deployment in 2012–2013, when concentrations over 400 μg L^{-1} were consistently observed (Meyer et al., 2022).

Our observed euphotic-zone POC magnitudes can be separated into three time periods (Figure 3b). Initial concentrations were ≈140 μg L^{-1} in early December and increased gradually until 3 January (green line in Figure 3), when POC increased abruptly reaching ≈ 200 μg L^{-1}. Relatively high POC continued until mid January (blue line), when it decreased until the survey end. Decreasing POC during the latter period is concomitant with the ongoing decrease in Chl-a after a relative peak in both variables (Figure 3a), and the presence of low-salinity surface meltwater lenses (Figures 2c and 3b) that induce strong stratification through the euphotic zone (orange line in Figure 3d). The high correlation ($R = 0.88$, $p<0.01$) between the POC:Chl-a ratio and stratification (black and orange lines respectively in Figure 3d) could be explained by growth of diatoms, with a higher POC:Chl-a ratio being favored in stratified, iron-depleted waters (Arrigo et al., 1998). Stratification peaks observed in late December and early January, before generalized presence of surface warm and fresh waters, could be related to mesoscale features entraining meltwater lenses in their surface (Figure 2c).

The temporal mean of the euphotic zone POC:Chl-a ratios exhibits exceptionally low values that ranged from 5.0 ± 2.4 in December to 19.5 ± 16.3 in January (Figures 2f and 3d), where the standard deviation represents the temporal variability. This contrasts with climatological POC:Chl-a ratios for the Ross Sea continental shelf of 129 ± 42 and 156 ± 47 for December and January respectively (Smith & Kaufman, 2018), and with those observed in previous glider deployments in the same Ross Sea area, namely 47 in December 2010 and 105 in January 2011 (Kaufman et al., 2014); 100–200 in December 2012 and 200–400 in January 2013 (Meyer et al., 2022).

3.2. Potential Drivers of the 2022–2023 Bloom

The satellite-derived incident PAR between 2002 and 2023 was generally greater in December than in January but in summer 2022–2023 it was similar for both (Figure 4a). This agrees with our incident PAR from the glider, whose means for December (65 μmol photon m^{-2} s^{-1}) and January (73 μmol photon m^{-2} s^{-1}) were similar (Figures 4a and S3a in Supporting Information S1). Interestingly, December 2022 was the second lowest climatological anomaly since the beginning of the satellite record in 2002 (Figure 4b). Photoacclimation of phytoplankton cells to low light conditions can enhance Chl-a, resulting in an increase in per cell Chl-a concentration that does not necessarily correspond to increased phytoplankton biomass (Graff et al., 2016). To date, culture experiments on Ross Sea phytoplankton have not shown evidence of photoacclimation under light conditions that were lower than we observed in our study (Alderkamp et al., 2019). Instead, Alderkamp et al. (2019) found that the most observed photoadaptative mechanism was photoinhibition to high irradiance. However, given that numerous studies have shown photoacclimation to be ubiquitous worldwide (e.g., Dubinsky and Stambler (2009); Graff et al. (2016)), we suggest that the particularly low-light conditions during summer in 2022–2023 (Figures 4a and 4b) might have resulted in photoacclimation partly accounting for the enhanced Chl-a concentrations. Moreover, the culture experiment from Alderkamp et al. (2019) showed a significant decrease in the POC:Chl-a ratio of Ross Sea phytoplankton under low light conditions, while these ratios were less affected by iron additions. Irradiance plays a role in regulating phytoplankton composition (Geider et al., 1997; Sunda & Huntaman, 1997), and in light-limited environments with enough iron, *Phaeocystis* generally dominates over diatoms. Thus, low-light conditions could explain the growth of *Phaeocystis* over diatoms until later than usual in our survey and also explain the correspondingly low POC:Chl-a ratios observed during summer 2022–2023 in the Ross Sea. At the scale of our survey, changes in stratification, often associated with iron depletion after the bloom maximum, could have also played a role in the transition in phytoplankton composition (Figure 3d) leading to the dissipation of *Phaeocystis* and allowing diatoms to grow.

Marginal ice zones in seasonally ice-covered Antarctic waters such as the Ross Sea are known to support large phytoplankton blooms as the sea ice melts (Smith & Nelson, 1985; Sedwick & Ditullio, 1997; Wilson et al., 1986) due to meltwater increasing stratification and thus biomass retention, and meltwater releasing bioavailable iron (Sedwick & Ditullio, 1997). Sea-ice cover in the study area was abnormally high during summer 2022–2023 (Figure 4). Most sea-ice melt occurred between 21 and 28 December (coinciding with the Chl-a peak), and until as late as the first half of January at the northern and western limits of the area covered by the gliders (Figure 1a). Taking into account the above factors, we hypothesize that a combination of increased stratification (Arrigo et al., 2017) and iron release from particularly late sea-ice melt, together with potential photoacclimation

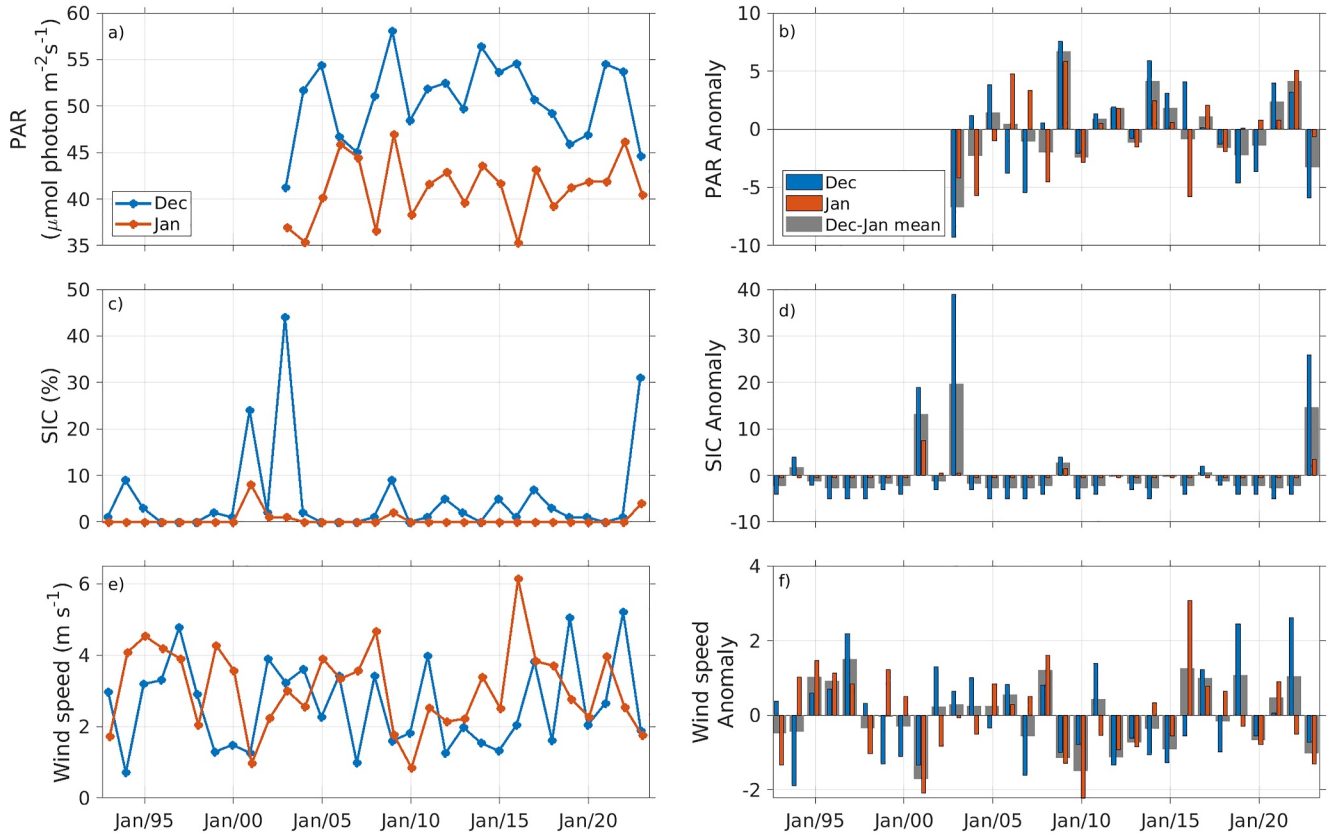

Figure 4. Time series between 1992 and 2023 in the region defined within the black rectangle in Figure 1a of (a) PAR (μmol photon m^{-2} s^{-1}) (b) PAR anomaly (μmol photon m^{-2} s^{-1}) (c) SIC) (%) (d) SIC anomaly (%) (e) Wind speed (m s^{-1}) (f) Wind speed anomaly (m s^{-1}). Anomalies were computed for each month by subtracting the 1992–2023 mean for that month.

to anomalously low-light, are the more plausible explanations for the extreme Chl-a concentrations observed during our survey. Monthly mean wind speeds during our survey were rather low (Figures 4e and 4f) but did not correlate with mixed layer depth (Figure 3e), which was largely determined by surface salinity (Figure 3b) and modulated by mesoscale features (Figure 2c). However, wind stress might have played an indirect role by influencing formation of mesoscale features or impacting sea-ice dynamics.

3.3. Uncertainties

While we are confident that both gliders independently captured an exceptionally large phytoplankton bloom, it is uncertain whether the high Chl-a values observed correspond entirely to an increase in biomass. For instance, lowered POC concentrations and the lack of a strong statistical relationship between POC and Chl-a raise questions about the overall biomass accumulation and POC export (Meyer et al., 2022). We cannot ensure that the calibration of chlorophyll fluorescence with extracted chlorophyll (the Fluorescence:Chl-a ratio) from water samples collected upon glider recovery can be extrapolated for the whole campaign. Fluorescence:Chl-a ratios in the Southern Ocean can change over time as result of species composition, nutrient limitation or pigment composition (Proctor & Roesler, 2010; Schallenberg et al., 2022). Iron limitation also can create high Fluorescence:Chl-a ratios in phytoplankton (Schallenberg et al., 2022). However, the Chl-a samples were collected during late January, when iron would have been at extremely low concentrations (Sedwick et al., 2011). Thus, Fluorescence:Chl-a ratios are not expected to be higher during the bloom peak, when iron was not yet fully consumed, than at the end. The latter suggests that our conversion of Chl-a fluorescence to Chl-a might be a lower bound for the whole mission, and that the phytoplankton bloom was truly unprecedented.

4. Summary and Conclusions

High temporal and spatial resolution observations from two Seagliders revealed an unprecedented, sustained phytoplankton bloom in the Ross Sea during austral summer 2022–2023. The high Chl-a concentrations that persisted for over a month and extended to depths of 100 m likely correspond to an ice-edge bloom fueled by iron release and relatively high stratification during an anomalously ice-covered December. We suggest that photoacclimation to low light conditions might have further enhanced Chl-a fluorescence. The timing of the sea-ice melt appeared to be critical for the bloom intensity by providing the perfect combination of iron availability, enough light, and high stratification. These conditions likely favored the initial growth of *Phaeocystis*, while the transition toward a diatom-dominated bloom, was correlated with an increased stratification.

The productivity of the Ross Sea is vulnerable to changes in sea-ice distribution and duration, as iron input from sea ice is critical in determining the magnitude of the summer bloom (Alderkamp et al., 2019). Despite experiencing important variations (Stammerjohn et al., 2012), sea-ice concentration and extent in the Ross Sea have generally increased over the past decades (Comiso et al., 2011; Farooq et al., 2020). However, future projections from regional modeling studies differ, with predictions of both an increase in sea-ice extent (DuVivier et al., 2024) and an expansion of the Ross Sea polynya (Smith, Dinniman, et al., 2014). In any scenario, climate-related changes such as increased seawater temperatures and changes in the wind strength (Jena et al., 2024; Smith, Dinniman, et al., 2014) will likely impact sea-ice cover, stratification, and/or iron supply. The latter would change iron limitation coping strategies and impact phytoplankton phenology and net primary productivity (Boyd et al., 2012). Thus, there is an urgent need to increase data-based knowledge of the interactions between the main phytoplankton bloom controls in this critical system that is the most productive region in the Southern Ocean. This is crucial for predicting potential consequences of climate change on regional food webs and carbon sequestration.

Data Availability Statement

The glider data used in this study (doi:10.5285/0a1c43b9-4738-75e0-e063-6c86abc0ea24) are available at (Portela et al., 2024) and from British Oceanographic Data Centre (BODC) https://www.bodc.ac.uk/data/published_data_library/catalogue/10.5285/0a1c43b9-4738-75e0-e063-6c86abc0ea24. The longterm SIC data can be found at (https://data.seaice.uni-bremen.de/amsr2/asi_daygrid_swath/s3125/). Wind speed data were obtained from ERA5 (Hersbach et al., 2018) at (https://cds.climate.copernicus.eu/cdsapp#!/dataset/reanalysis-era5-single-levels?tab=overview), and satellite AQUA-MODIS PAR data (NASA Ocean Biology Processing Group, 2018) can be found here https://oceandata.sci.gsfc.nasa.gov/directdataaccess/Level-3%20Binned/Aqua-MODIS.

Acknowledgments
We thank the Natural Environment Research Council (NERC), National Science Foundation (NSF), and McMurdo Station staff for funding and logistical support. The authors were supported by NSFGEO-NERC collaborative project P2P: Plankton to Predators—Biophysical Controls in Antarctic Polynyas (PI David Ainley, NSF grant ANT-2040571 and NERC grant NE/W00755X/1). The glider campaign was further supported by COMPASS: Climate-relevant Ocean Measurements and Processes on the Antarctic Continental Shelf and Slope (European Research Council, Horizon 2020: Grant 741120). We thank Gillian Damerell and Gareth Lee for their work in glider deployment and set up, and the UEA glider science team for glider piloting.

References

Alderkamp, A. C., Dijken, G. L. V., Lowry, K. E., Lewis, K. M., Joy-Warren, H. L., Poll, W. V. D., et al. (2019). Effects of iron and light availability on phytoplankton photosynthetic properties in the ross sea. *Marine Ecology Progress Series*, *621*, 33–50. https://doi.org/10.3354/meps13000

Arrigo, K. R., Robinson, D. H., Worthen, D. L., Dunbar, R. B., DiTullio, G. R., VanWoert, M., & Lizotte, M. P. (1999). Phytoplankton community structure and the drawdown of nutrients and CO2 in the Southern Ocean. *Science*, *283*(5400), 365–367. https://doi.org/10.1126/science.283.5400.365

Arrigo, K. R., & van Dijken, G. L. (2003). Phytoplankton dynamics within 37 antarctic coastal polynya systems. *Journal of Geophysical Research*, *108*(C8). https://doi.org/10.1029/2002jc001739

Arrigo, K. R., van Dijken, G. L., Alderkamp, A. C., Erickson, Z. K., Lewis, K. M., Lowry, K. E., et al. (2017). Early spring phytoplankton dynamics in the western antarctic peninsula. *Journal of Geophysical Research: Oceans*, *122*(12), 9350–9369. https://doi.org/10.1002/2017JC013281

Arrigo, K. R., van Dijken, G. L., & Bushinsky, S. (2008). Primary production in the Southern Ocean, 1997-2006. *Journal of Geophysical Research*, *113*(C8), 1997–2006. https://doi.org/10.1029/2007JC004551

Arrigo, K. R., Weiss, A. M., & Smith, W. O. (1998). Physical forcing of phytoplankton dynamics in the southwestern Ross Sea. *Journal of Geophysical Research*, *103*(C1), 1007–1021. https://doi.org/10.1029/97jc02326

Boyd, P. W. (2002). Environmental factors controlling phytoplankton processes in the Southern Ocean. *Journal of Phycology*, *38*(5), 844–861. https://doi.org/10.1046/j.1529-8817.2002.t01-1-01203.x

Boyd, P. W., Arrigo, K. R., Strzepek, R., & Dijken, G. L. V. (2012). Mapping phytoplankton iron utilization: Insights into Southern Ocean supply mechanisms. *Journal of Geophysical Research*, *117*(C6). https://doi.org/10.1029/2011JC007726

Comiso, J. C., Kwok, R., Martin, S., & Gordon, A. L. (2011). Variability and trends in sea ice extent and ice production in the Ross Sea. *Journal of Geophysical Research*, *116*(C4), C04021. https://doi.org/10.1029/2010JC006391

DiTullio, G. R., Geesey, M. E., Leventer, A., & Lizotte, M. P. (2003). Algal pigment ratios in the Ross Sea: Implications for Chemtax analysis of Southern Ocean data. Biogeochemistry of the Ross Sea. *Atarctic Research Series*, *78*, 35–52. https://doi.org/10.1029/078ars03

Dubinsky, Z., & Stambler, N. (2009). Photoacclimation processes in phytoplankton: Mechanisms, consequences, and applications. *Aquatic Microbial Ecology*, *56*, 163–176. https://doi.org/10.3354/ame01345

DuVivier, A. K., Molina, M. J., Deppenmeier, A. L., Holland, M. M., Landrum, L., Krumhardt, K., & Jenouvrier, S. (2024). Projections of winter polynyas and their biophysical impacts in the Ross Sea Antarctica. *Climate Dynamics*, *62*(2), 989–1012. https://doi.org/10.1007/s00382-023-06951-z

Farooq, U., Rack, W., McDonald, A., & Howell, S. (2020). Long-term analysis of sea ice drift in the western Ross sea, Antarctica, at high and low spatial resolution. *Remote Sensing*, *12*(9), 1402. https://doi.org/10.3390/RS12091402

Frajka-Williams, E., Eriksen, C. C., Rhines, P. B., & Harcourt, R. R. (2011). Determining vertical water velocities from Seaglider. *Journal of Atmospheric and Oceanic Technology*, *28*(12), 1641–1656. https://doi.org/10.1175/2011JTECHO830.1

Garau, B., Ruiz, S., efeng G Hang, W., Pascual, A., Heslop, E., Kerfoot, J., & Tintoré, J. (2011). Thermal lag correction on slocum ctd glider data. *Journal of Atmospheric and Oceanic Technology*, *28*(9), 1065–1071. https://doi.org/10.1175/JTECH-D-10-05030.1

Gardner, W. D., Richardson, M. J., & Smith, W. O. (2000). Seasonal patterns of water column particulate organic carbon and fluxes in the Ross Sea, Antarctica. *Deep-Sea Research II*, *47*(15–16), 3423–3449. https://doi.org/10.1016/s0967-0645(00)00074-6

Geider, R., MacIntyre, H., & Kana, T. (1997). Dynamic model of phytoplankton growth and acclimation: Responses of the balanced growth rate and the chlorophyll a:carbon ratio to light, nutrient-limitation and temperature. *Marine Ecology: Progress Series*, *148*, 187–200. https://doi.org/10.3354/meps148187

Goffart, A., Catalano, G., Hecq, J. H., & Belgium, B. (2000). Factors controlling the distribution of diatoms and Phaeocystis in the Ross Sea. *Journal of Marine Systems*, *27*(1–3), 161–175. https://doi.org/10.1016/s0924-7963(00)00065-8

Graff, J. R., Westberry, T. K., Milligan, A. J., Brown, M. B., Dall'Olmo, G., Reifel, K. M., & Behrenfeld, M. J. (2016). Photoacclimation of natural phytoplankton communities. *Marine Ecology Progress Series*, *542*, 51–62. https://doi.org/10.3354/meps11539

Hersbach, H., Bell, B., Berrisford, P., Biavati, G., Horányi, A., Sabater, J. M., et al. (2018). ERA5 hourly data on single levels from 1940 to present. *Copernicus Climate Change Service (C3S) Climate Data Store (CDS)*. [dataset]. https://doi.org/10.24381/cds.adbb2d47

Jena, B., Kshitija, S., Bajish, C. C., Turner, J., Holmes, C., Wilkinson, J., et al. (2024). Evolution of antarctic sea ice ahead of the record low annual maximum extent in September 2023. *Geophysical Research Letters*, *51*(7). https://doi.org/10.1029/2023GL107561

Jones, R. M., & Smith, W. O. (2017). The influence of short-term events on the hydrographic and biological structure of the southwestern Ross Sea. *Journal of Marine Systems*, *166*, 184–195. https://doi.org/10.1016/j.jmarsys.2016.09.006

Kaufman, D. E., Friedrichs, M. A. M., Smith, W. O., Queste, B. Y., & Heywood, K. J. (2014). Biogeochemical variability in the southern ross sea as observed by a glider deployment. *Deep-Sea Research Part I Oceanographic Research Papers*, *92*, 93–106. https://doi.org/10.1016/j.dsr.2014.06.011

Knap, A., Michaels, A., Close, A., Ducklow, H., & Dickson, A. (1996). Protocols for the joint global ocean flux study (JGOFS) core measurements. Retrieved from http://www.wetlabs.com/iopdescript/attenintro.htm.*19*

McGillicuddy, D. J., Sedwick, P. N., Dinniman, M. S., Arrigo, K. R., Bibby, T. S., Greenan, B. J., et al. (2015). Iron supply and demand in an Antarctic shelf ecosystem. *Geophysical Research Letters*, *42*(19), 8088–8097. https://doi.org/10.1002/2015GL065727

Meier, W. N., Fetterer, F., Windnagel, A. K., & Stewart, J. S. (2021). Near-real-time NOAA/NSIDC climate data record of passive microwave sea ice concentration, version 2. [Dataset]. https://doi.org/10.7265/tgam-yv28

Meyer, M. G., Jones, R. M., & Smith, W. O. (2022). Quantifying seasonal particulate organic carbon concentrations and export potential in the southwestern Ross Sea using autonomous gliders. *Journal of Geophysical Research: Oceans*, *127*(10), 1–15. https://doi.org/10.1029/2022JC018798

Müller, P., Li, X.-P., & Niyogi, K. K. (2001). Update on photosynthesis non-photochemical quenching. *A Response to Excess Light Energy*. Retrieved from www.plantphysiol.org

NASA Ocean Biology Processing Group. (2018). Seawifs-orbview-2 level 2 ocean color data version r2018.0. *NASA Ocean Biology Distributed Active Archive Center*. [dataset]. https://doi.org/10.5067/ORBVIEW-2/SEAWIFS/L2/OC/2018

Portela, E., Heywood, K. J., Damerell, G., Smith, W. O., Meyer, M. G., & Lee, G. (2024). Seaglider data from the western Ross Sea, Antarctica, November 2022-January 2023. *NERC EDS British Oceanographic Data Centre NOC*. [Dataset]. https://doi.org/10.5067/ORBVIEW-2/SEAWIFS/L2/OC/2018

Proctor, C. W., & Roesler, C. S. (2010). New insights on obtaining phytoplankton concentration and composition from in situ multispectral chlorophyll fluorescence. *Limnology and Oceanography: Methods*, *8*, 695–708. https://doi.org/10.5285/0a1c43b9-4738-75e0-e063-6c86abc0ea24

Queste, B. Y., Heywood, K. J., Smith, W. O., Kaufman, D. E., Jickells, T. D., & Dinniman, M. S. (2014). Dissolved oxygen dynamics during a phytoplankton bloom in the Ross Sea polynya. *Antarctic Science*, *27*(4), 362–372. https://doi.org/10.1017/S0954102014000881

Rozema, P. D., Venables, H. J., van de Poll, W. H., Clarke, A., Meredith, M. P., & Buma, A. G. (2017). Interannual variability in phytoplankton biomass and species composition in northern Marguerite Bay (West Antarctic Peninsula) is governed by both winter sea ice cover and summer stratification. *Limnology & Oceanography*, *62*(1), 235–252. https://doi.org/10.1002/lno.10391

Ryan-Keogh, T. J., & Smith, W. O. (2021). Temporal patterns of iron limitation in the Ross Sea as determined from chlorophyll fluorescence. *Journal of Marine Systems*, *215*, 103500. https://doi.org/10.1016/j.jmarsys.2020.103500

Salmon, E., Hofmann, E. E., Dinniman, M. S., & Smith, W. O. (2020). Evaluation of iron sources in the Ross Sea. *Journal of Marine Systems*, *212*, 103429. https://doi.org/10.1016/j.jmarsys.2020.103429

Schallenberg, C., Strzepek, R. F., Bestley, S., Wojtasiewicz, B., & Trull, T. W. (2022). Iron limitation drives the globally extreme fluorescence/chlorophyll ratios of the Southern Ocean. *Geophysical Research Letters*, *49*(12). https://doi.org/10.1029/2021GL097616

Sedwick, P. N., & Ditullio, G. R. (1997). Regulation of algal blooms in antarctic shelf waters by the release of iron from melting sea ice. *Geophysical Research Letters*, *24*(20), 2515–2518. https://doi.org/10.1029/97GL02596

Sedwick, P. N., Marsay, C. M., Sohst, B. M., Aguilar-Islas, A. M., Lohan, M. C., Long, M. C., et al. (2011). Early season depletion of dissolved iron in the Ross Sea polynya: Implications for iron dynamics on the Antarctic continental shelf. *Journal of Geophysical Research*, *116*(C12), C12019. https://doi.org/10.1029/2010JC006553

Smith, W. O. (2022). Primary productivity measurements in the Ross Sea, Antarctica: A regional synthesis. *Earth System Science Data*, *14*(6), 2737–2747. https://doi.org/10.5194/essd-14-2737-2022

Smith, W. O., Ainley, D. G., Arrigo, K. R., & Dinniman, M. S. (2014). The oceanography and ecology of the Ross Sea. *Annual Review of Marine Science*, *6*(1), 469–487. https://doi.org/10.1146/annurev-marine-010213-135114

Smith, W. O., Asper, V., Tozzi, S., Liu, X., & Stammerjohn, S. E. (2011). Surface layer variability in the Ross Sea, Antarctica as assessed by in situ fluorescence measurements. *Progress in Oceanography*, *88*(1–4), 28–45. https://doi.org/10.1016/j.pocean.2010.08.002

Smith, W. O., Dinniman, M. S., Hofmann, E. E., & Klinck, J. M. (2014). The effects of changing winds and temperatures on the oceanography of the Ross Sea in the 21st century. *Geophysical Research Letters*, *41*(5), 1624–1631. https://doi.org/10.1002/2014GL059311

Smith, W. O., & Jones, R. M. (2015). Vertical mixing, critical depths, and phytoplankton growth in the Ross Sea. *ICES Journal of Marine Science*, *72*(6), 1952–1960. https://doi.org/10.1093/icesjms/fsu234Contribution

Smith, W. O., & Kaufman, D. E. (2018). Climatological temporal and spatial distributions of nutrients and particulate matter in the Ross Sea. *Progress in Oceanography*, *168*, 182–195. https://doi.org/10.1016/j.pocean.2018.10.003

Smith, W. O., Marra, J., Hiscock, M. R., & Barber, R. T. (2000). The seasonal cycle of phytoplankton biomass and primary productivity in the Ross Sea, Antarctica. *Deep-Sea Research Part II Topical Studies in Oceanography*, *47*(15–16), 3119–3140. https://doi.org/10.1016/S0967-0645(00)00061-8

Smith, W. O., & Nelson, D. M. (1985). Phytoplankton bloom produced by a receding ice edge in the Ross Sea: Spatial coherence with the density field. *Science*, *227*(4683), 163–166. https://doi.org/10.1126/science.227.4683.163

Smith, W. O., & Trimborn, S. (2024). Annual review of marine science Phaeocystis: A global enigma. *Annual Review ofMarine Science*, *16*(1), 417–441. https://doi.org/10.1146/annurev-marine-022223

Spreen, G., Kaleschke, L., & Heygster, G. (2008). Sea ice remote sensing using amsr-e 89-ghz channels. *Journal of Geophysical Research*, *113*(C2). https://doi.org/10.1029/2005JC003384

Stammerjohn, S., Massom, R., Rind, D., & Martinson, D. (2012). Regions of rapid sea ice change: An inter-hemispheric seasonal comparison. *Geophysical Research Letters*, *39*(6). https://doi.org/10.1029/2012GL050874

Strzepek, R. F., Maldonado, M. T., Hunter, K. A., Frew, R. D., & Boyd, P. W. (2002). Adaptive strategies by Southern Ocean phytoplankton to lessen iron limitation: Uptake of organically complexed iron and reduced cellular iron requirements. *Limnology & Oceanography*, *56*(6), 1983–2002. https://doi.org/10.4319/lo.2011.56.6.1983

Sunda, W. G., & Huntaman, S. A. (1997). Interrelated influence of iron, light and cell size on marine phytoplankton growth. *Nature*, *390*(6658), 389–392. https://doi.org/10.1038/37093

Wilson, D. L., Smith, W. O., & Nelson, D. M. (1986). Phytoplankton bloom dynamics of the western Ross Sea ice edge-I. Primary productivity and species-specific production. *Deep-Sea Research, Part A: Oceanographic Research Papers*, *33*(10), 1375–1387. https://doi.org/10.1016/0198-0149(86)90041-5

Xing, X., Briggs, N., Boss, E., & Claustre, H. (2018). Improved correction for non-photochemical quenching of in situ chlorophyll fluorescence based on a synchronous irradiance profile. *Optics Express*, *26*(19), 24734. https://doi.org/10.1364/oe.26.024734

Yuan, N., Ding, M., Ludescher, J., & Bunde, A. (2017). Increase of the antarctic sea ice extent is highly significant only in the Ross Sea. *Scientific Reports*, *7*(1), 41096. https://doi.org/10.1038/srep41096

References From the Supporting Information

Boss, E., & Pegau, W. S. (2001). Relationship of light scattering at an angle in the backward direction to the backscattering coefficient. *Applied Optics*, *40*(30), 5503. https://doi.org/10.1364/ao.40.005503

Morel, A., Huot, Y., Gentili, B., Werdell, P. J., Hooker, S. B., & Franz, B. A. (2007). Examining the consistency of products derived from various ocean color sensors in open ocean (case 1) waters in the perspective of a multi-sensor approach. *Remote Sensing of Environment*, *111*(1), 69–88. https://doi.org/10.1016/j.rse.2007.03.012

Saulquin, B., Hamdi, A., Gohin, F., Populus, J., Mangin, A., & d'Andon, O. F. (2013). Estimation of the diffuse attenuation coefficient kdpar using meris and application to seabed habitat mapping. *Remote Sensing of Environment*, *128*, 224–233. https://doi.org/10.1016/j.rse.2012.10.002